Cymantrene–triazole "Click" Products: Structural Characterization and Electrochemical Properties

David P. Day,[a] Thomas Dann,[a] David. L. Hughes,[a] Vasily. S. Oganesyan,[a] Dietmar Steverding,[b]

Gregory G. Wildgoose*[a]

[a] Energy & Materials Laboratory, School of Chemistry, University of East Anglia, Norwich Research Park, Norwich, NR4 7TJ, United Kingdom

[b] BioMedical Research Centre, Norwich Medical School, University of East Anglia, Norwich Research Park, Norwich NR4 7TJ, United Kingdom

Supporting Information Placeholder

ABSTRACT: We report the first known examples of triazole-derivatised cymantrene complexes (η^5-[4-substituted-triazol-1-yl]cyclopentadienyl tricarbonyl manganese(I), obtained *via* a "click" chemical synthesis, bearing either a phenyl, 3-aminophenyl or 4-aminophenyl moiety at the 4-position of the triazole ring. Structural characterization data using multinuclear NMR, UV-vis, ATR–IR and mass spectrometric methods are provided as well as crystallographic data for (η^5-[4-phenyltriazol-1-yl]cyclopentadienyl tricarbonyl manganese(I) and (η^5-[4-(3-aminophenyl)triazol-1-yl]cyclopentadienyl tricarbonyl manganese(I). Cyclic voltammetric characterization of the redox behaviour of each of the three cymantrene–triazole complexes is presented together with digital simulations, *in situ* infra-red spectroelectrochemistry and DFT calculations to extract the associated kinetic and thermodynamic parameters. The trypanocidal activity of each cymantrene-triazole complex is also examined and found to be more active than cymantrene alone.

1. Introduction

The chemistry of cymantrene [(η^5-C_5H_5)Mn(CO)$_3$], **1**, has most recently been reported across a variety of chemical disciplines. Recently it has found applications in photochemical studies[1] and hydrogen generation *via* water splitting reactions.[2] Cymantrene derivatives have been combined with known antimalarial drugs such as chloroquine,[3] and have been tested for antiproliferative activity against breast cancer cell lines,[4] to highlight just a few of its many chemical applications.

Geiger has recently reviewed the redox chemistry of various piano-stool complexes, including cymantrene **1**,[5] and was the first to report the anodic one-electron oxidation of cymantrene and its use as an oxidative redox tag to rival the more commonly used ferrocenyl redox tags.[6] Geiger demonstrated that, upon electrochemical oxidation, the cymantrene radical cation could be generated in a CH_2Cl_2 solution of [^{n}Bu$_4$N][B(C_6F_5)$_4$] electrolyte, and was sufficiently long-lived to allow the collection of spectral characterization data. However, the electrogenerated cymantrene radical cation is sufficiently reactive that it will undergo unwanted side reactions with common electrolyte salts (such as [^{n}Bu$_4$N][PF_6]). Therefore, in order to obtain meaningful voltammetric data, Geiger advocates the use of weakly coordinating anion electrolytes such as [^{n}Bu$_4$N][B(C_6F_5)$_4$] together with weakly donor solvents such as dichloromethane.[7]

In 2010, Geiger introduced a number of sandwich and half-sandwich organometallic complexes that contain a cyclopentadienyldiazonium moiety that are capable of undergoing a one-electron reduction, to generate a cyclopentadienyl-based radical that can then form a covalent bond to a glassy carbon electrode.[8] Our ultimate goal is to exploit the redox properties of analogues of cymantrene, **1**, when covalently bound to an electrode surface by a "molecular linker" spacer unit; and a target linker could potentially be a triazole moiety formed *via* facile "click" reactions.

The most powerful "click" chemistry reaction to date to affording 5-membered heterocycles is probably the copper-catalyzed variant of the Huisgen 1,3-dipolar cycloaddition.[9] The 1,4-copper catalyzed azide-alkyne "click" reaction (CuAAC) has been extensively reviewed, and utilizing such an approach would adhere to stringent criteria as set by Nobel laureate, Barry Sharpless.[10] Most recently, the "click" reaction has become a topic of considerable interest in the coordination chemistry of metal complexes, for example: 2-pyridyl-1,2,3-triazole ligands have been used in the formation of various new transition-metal coordination complexes,[11] and, a similar approach was reported for the generation of new iridium(III) and ruthenium(II) complexes coordinating these pyridyl-triazole ligands.[12] Tripodal-triazole ligands have also been reported to coordinate various transition-metals.[13]

To date, the application of "click" reactions to organometallic sandwich and half-sandwich complexes, has, in most cases, been limited to ferrocene and derivatives thereof. These modified ferrocene-triazole products have been utilized for a number of important applications. Molina and co-workers have shown that the "click" reaction can be utilized to generate an assortment of ferrocene-triazole click products, all of which are excellent electrooptical ion pair recognition receptors.[14] Astruc and co-workers have reported the modification of dendrimers that act as sensors that recognize both oxoanions and transition-metal cations.[15] Astruc was also the first to report the modification of dendrimers with cobaltocene *via* a click chemistry reaction, having similar applications to their ferrocene counterparts.[16] The synthesis of permetalated alkyne-

azide "click" cycloadducts has recently been reported by Gladysz and co-workers, showing that the click reaction can also be applied to half-sandwich metal carbonyl complexes, in this case utilizing a new rhenium cyclopentadienylazide complex.[17]

To our surprise, we are as yet unaware of any reports that modify cymantrene, **1**, with 1,4-disubstituted-1,2,3-triazole moieties. To address this, we herein present structural characterization data for three new cymantrene-triazole complexes, starting from the cymantrene azide, **2**, such that the cymantrene moiety is maintained at the 1-position of the triazole ring. These model complexes also bear a phenyl, **3**, 4-aminophenyl, **4**, or 3-aminophenyl, **5**, substituent attached to the carbon atom at the 4-position of the triazole ring (Scheme 1). We also report the solution–phase redox chemistry of these new complexes obtained using cyclic voltammetry, together with relevant mechanistic, kinetic, and thermodynamic parameters obtained by digital simulation of experimental voltammetric data. Furthermore, complexes **4** and **5** are prototypical precursors for surface modification reactions *via* diazonium salt formation and electrolytic reduction.

2. Results and Discussion

2.1 Synthesis and structural characterization

In our approach to synthesizing various triazole–derivatised cymantrene complexes, we identified two potential retro–synthetic starting points, either: derivatizing the cyclopentadiene ring with a pendant alkyne group; or derivatising the cyclopentadiene ring with an azide group. We note that Geiger has recently introduced pendant alkyne groups into cymantrene complexes and used these as linkers for surface attachment[18] whilst Holovics[19] and Sünkel[20] have both previously reported the synthesis of cymantrenyl azide **3** in good yields, and in each case, handled the product as a crude mixture to be used in subsequent synthetic steps. Given that our ultimate aim is to form organometallic-triazoles for electrode surface modification, we opted for the latter approach, starting from the cymantrene azide, **2**, for several reasons. First, following the recent work of Downard,[21] generating an azide on the organometallic complex requires the electrode to be derivatised *via* reduction of aryl-alkyne diazonium salts which are easier to handle and more stable than the alternative aryl-azide diazonium salts. Second, having the alkyne unit bound to the electrode surface as opposed to an azide moiety reduces the opportunity for undesirable side reactions during the coupling reaction.[22]

We report the synthesis of **2** as a light brown solid in good yield (75:25 of **2**:**1**, Scheme 1) which can be used directly in the following steps.[23] Our first attempt at the copper-catalyzed azide/alkyne cycloaddition of **3** was achieved using modified conditions as proposed by Hu *et al* (Scheme 1).[24] Reassuringly, the transformation of **2** into **3** was complete in 2 hours under these mild conditions; purification of **3** *via* silica gel flash column chromatography afforded **3** as a yellow solid in excellent yield and high purity (Scheme 1).

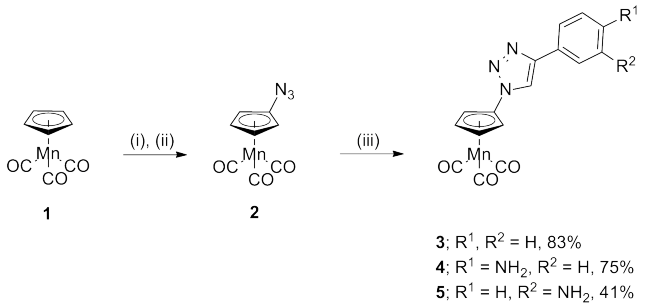

Scheme 1. *Reagents and conditions*: (i) **1** (1 equivalent), *n*-BuLi (1 equivalent), THF, -78 °C, 2 h; (ii) *p*-toluenesulfonylazide (1 equivalent), THF, -78 °C – rt, 14 h. (iii) **2** (1 equivalent), phenylacetylene (1 equivalent for **3**), or 4-ethynylaniline (1 equivalent for **4**), or 3-ethynylaniline (1 equivalent for **5**), $Cu(OAc)_2.H_2O$ (0.1 equivalent), CH_3CN, 2-4 h.

The ^{1}H NMR spectrum of **3** allows us to assign the key areas of the complex, confirming that our product was indeed the desired cymantrene-click based product. We observe a characteristic splitting of the five protons in the cyclopentadienyl ligand observed as a singlet in **1**, into two equivalent triplets integrating to two protons each for the cyclopentadienyl protons of complex **3** (δ 4.8-5.5 ppm), formed by the introduction of a single triazole moiety. ^{1}H COSY NMR experiments have shown the aromatic protons of the phenyl substituent attached to the triazole moiety can couple to one another around the region of δ 7.3-7.9 ppm. The proton at the 5-position of the triazole moiety is observed as a singlet at δ 7.99 ppm (see Supporting Information Figure S3).

The UV-vis spectra of the parent molecule, $CpMn(CO)_3$, **1**, can be directly compared with click-product **3**, and we show that in both cases, we observe MLCT bands around the region of 330-340 nm. We attribute these absorptions to an MLCT band, based on closely related systems to our cymantrene complexes (see Supporting Information Figure S6).[25]

The infra-red spectral data collected for compounds **1**-**5**, with band assignments, are tabulated below (Table 1, See Figures S7 (a)–(e) for IR spectra of compounds **1**-**5**).

Table 1. (ν/cm^{-1}) Bands for complexes **1**-**5**

Complex	ν (C≡O)/cm^{-1}		ν(C=C) (triazole) /cm^{-1}
	sym	asym	
1	2014	1905	n/a
2	2016	1910	n/a
3	2024	1959, 1936, 1918	1533
4	2022	1940, 1910	1622, 1566, 1540
5	2022	1928	1614, 1592, 1530

Each of the three new cymantrene-triazole complexes, **3**-**5**, exhibit both symmetric and asymmetric metal–carbonyl stretches at *ca.* 2020 cm^{-1} and 1920-1940 cm^{-1} respectively.[6] Each complex also exhibits key infrared stretches in the region of 1500-1600 cm^{-1}, which we assign to the triazole C=C bond stretching modes in our complexes by comparison to previous literature reports.[13,26]

Further purification of **3** *via* slow recrystallization from petroleum (50:50) ether:dichloromethane yields colorless plates suitable for X-ray crystallography. Crystal structure analysis confirms that **3** contains the 1,4-disubstituted triazole ligand. There are two independent molecules in the crystal (Figure 1), and these lie adjacent, about 3.4 Å apart and related by a pseudo-centre of symmetry. The normals to the central triazole rings in the two molecules are 1.1(3)° apart.

The manganese atoms are coordinated by three carbonyl groups and the cyclopentadienyl (Cp) group of the triazole ligand, in a three-legged piano stool arrangement. The three rings of each triazole ligand are approximately coplanar, with the normal to the triazole ring rotated 14.0(3)° from the normal to the Cp ring and 12.2(2)° from that to the phenyl ring in the first ligand and, correspondingly, 12.9(3)° and 10.6(3)° in the second molecule.

The triazole ligands of the molecules of Mn(1) and Mn(2) overlap with N(6) above the centre of the neighbouring phenyl ring, and N(1) below the opposite phenyl ring. The overlaps of the next ligands are more offset, with the normals of adjacent triazole rings 17.0(2)° apart. The alignment of these ligands can be seen in the packing diagram, Figure 2.

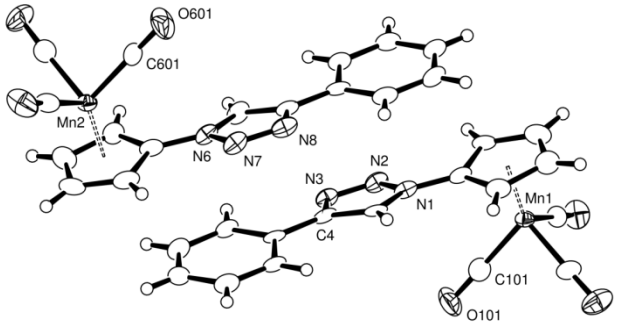

Figure 1. The two independent molecules in crystals of compound **3**. Thermal ellipsoids are shown at the 50% probability level. Mean Mn-C(carbonyl) and Mn-C(cp) bond lengths are 1.796(6) and 2.147(13) Å.

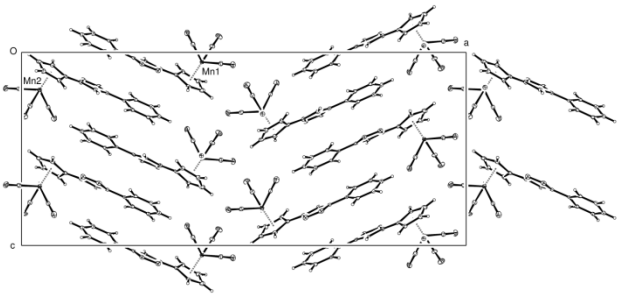

Figure 2. The crystal packing of **3**, viewed down the short *b* axis.

Looking at the ligand bond lengths in complex **3**, we observe the mean Mn-C(carbonyl) average bond length to be 1.796 (6) Å. When comparing this to the known Mn-C(carbonyl) bond length values from the literature for cymantrene, **1**, our value (1.796 (6) Å) is similar to that reported by Borissova *et al.*,[27] who observe the Mn-CO average bond length to be 1.797 (4) Å. We can also compare the mean Mn-C(cyclopentadienyl) bond lengths between complex **3** (2.147 (4) Å), to that of the known complex cymantrene, **1**, (2.145 (5) Å), showing again the values are almost identical.

Numerous literature reports demonstrate that organic triazole compounds are formed in high yield using the 1,4-CuAAC reaction when the phenylalkyne substrate bears an unprotected primary amine groups on the aromatic ring.[28,29] To extend our synthetic approach further, we sought to incorporate an amine group into the pendant aryl ring of the cymantrene–triazole, as a useful synthetic handle for future covalent surface attachment. We attempted the formation of 1,4-disubstituted triazole, **4**, under similar conditions to those for **3**. Reassuringly, the reaction was complete after 4 hours. After purification *via* silica gel flash column chromatography, Click-product **4** was formed in 88% yield as a fine yellow powder. This material stubbornly resisted attempts to grow X-ray quality crystals from a wide variety of solvent mixtures, thus preventing X-ray crystallographic analysis. However, confirmation of the cymantrene-click product **4** was shown through ^{1}H and ^{13}C NMR characterization amongst other forms of analysis (see Supporting Information Figure S4).

The 1,4-disubstituted triazole **5** containing an amine moiety at the *meta*-position of the phenyl ring was synthesized in a much lower yield than that observed for **4**. However, after purification *via* silica gel flash column chromatography, **5** was isolated as a dark yellow oil. Compound **5** was crystallized by slow evaporation from a mixture of dichloromethane-petroleum ether to yield **5** as colorless shards suitable for X-ray analysis (Figure 3). Crystal structure analysis confirms that **5** contains the 1,4-disubstituted triazole ligand.

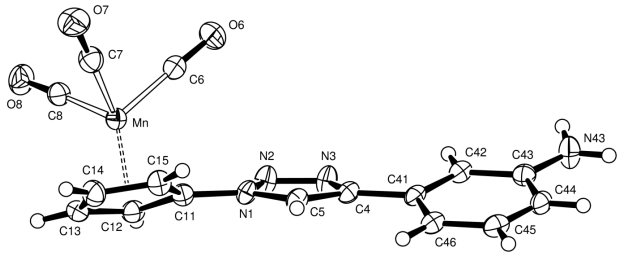

Figure 3. View of a molecule of (η^5-[4-(3-aminophenyl)triazol-1-yl]cyclopentadienyl tricarbonyl manganese(I) **5**, indicating the atom numbering scheme. Thermal ellipsoids are drawn at the 50% probability level.

Analysis of the crystal structure of **5** shows the manganese atom lies 1.774(2) Å from the mean-plane of the Cp ring atoms (Figure 3), and the three carbonyl ligands are arranged in an almost tripodal pattern on the opposite side of the metal; the mean C_{CO}–Mn–C_{CO} angle is 91.7°.

The three rings form a progression in orientation by rotation; about the C(11)–N(1) bond, the normals to the Cp and triazole rings are 26.0(2)° apart and the corresponding rotation about the C(4)–C(41) bond is 16.2(2)° in the same direction (Figure 3). There are no close contacts of the amino group, and nothing close enough to indicate any hydrogen bonding interactions.

There are π…π interactions between offset overlapping of phenyl rings *ca* 3.45 Å apart, around centres of symmetry (Figure 4). The parallel

alignments of pairs of triazole rings are further apart, at *ca* 3.63 Å. The closest intermolecular contact is of a triazole C(12)–H(12) group pointing to the edge of a phenyl ring with H(12) ... C(46') 2.78 Å.

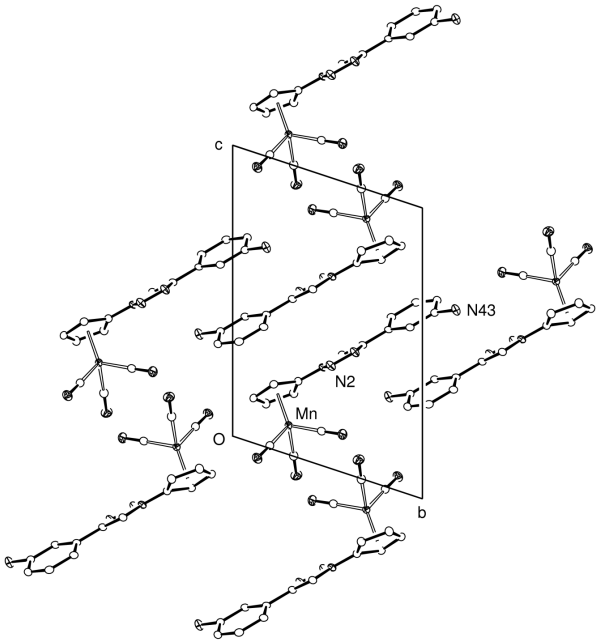

Figure 4. Crystal packing of molecules of (η^5-[4-(3-aminophenyl)triazol-1-yl]cyclopentadienyl tricarbonyl manganese (I) **5**.

We were curious to see the changes in bond lengths in the triazole ligand of complexes **3** and **5** when compared directly with the known crystal data for the model, free triazole ligand, as reported by Elguero *et al.* (4(5)-phenyl-1,2,3-triazole, **6**).[30] Average bond lengths for the metal-triazole complexes **3** and **5** and the free triazole **6** are tabulated below (Table 2). There are two small interesting differences observed when comparing the organometallic triazole complexes **3** and **5** to the known free triazole ligand **6**; The bond length N3-C4 in the free triazole **6** is 0.04-0.05 Å shorter than the two manganese-triazole complexes **3** and **5**; the same difference is observed for the N1-N2 bond length, where the free triazole **6** is *ca*. 0.04 Å shorter than the two manganese-triazole complexes **3** and **5**.

Table 2. Mean bond lengths [Å] for compounds **3**, **5** and **6**. Esd are given in parentheses.

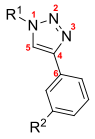

3; R^1 = $CpMn(CO)_3$, R^2 = H
5; R^1 = $CpMn(CO)_3$, R^2 = NH_2
6; R^1 = H, R^2 = H

Bond	Compound		
	3	**5**	**6**
N1-N2	1.356 (6)	1.353 (4)	1.315 (3)
N2-N3	1.325 (7)	1.311 (4)	1.321 (3)
N3-C4	1.383 (6)	1.371 (4)	1.332 (3)
C4-C5	1.384 (7)	1.375 (4)	1.386 (3)
C5-N1	1.341 (6)	1.358 (4)	1.325 (3)
C4-C6	1.476 (7)	1.471 (4)	1.472 (3)

Having synthesized and structurally characterized compounds **3-5**, we now focus on characterizing their redox chemistry.

2.2 Cyclic voltammetric characterization

We first investigated the electrochemical properties of **3** (2 mM), in dichloromethane containing 0.1M [^{n}Bu$_4$N][B(C$_6$F$_5$)$_4$] as supporting electrolyte, using cyclic voltammetry (CV, Figure 5, and Figure S8).

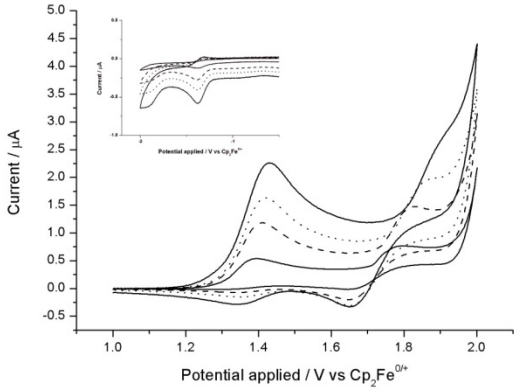

Figure 5. Cyclic voltammogram recorded for 2 mM (η^5-[4-phenyltriazol-1-yl]cyclopentadienyl tricarbonyl manganese(I) **3** in CH_2Cl_2 over the oxidative region at varied scan rates (solid line = 2000 mV s^{-1} ; dotted line = 1000 mV s^{-1}; dashed line = 500 mV s^{-1}; 2nd solid line = 100 mV s^{-1}). Inset: the corresponding scans over the reductive region (see text).

Analysis of the cyclic voltammogram reveals two oxidations at +1.400 V and +1.775 V *vs* ferrocene. By comparison with the voltammetry of 1,4-diphenyltriazole (our organic model for the triazole unit) we can assign the first oxidation wave to the cymantrene/cymantrene$^{+\cdot}$ redox couple, and the second to the quasi-reversible oxidation of the triazole/triazolium redox couple. At slow scan rates the cymantrene oxidation appears irreversible, but a small reduction wave is observable in the reverse scan at faster scan rates. This is indicative of the cymantrene radical cation undergoing a subsequent chemical reaction (*vide infra*). If the potential window is extended into the reductive region an irreversible reduction with surface adsorbed character is observed at *ca* -0.315 V and an electrochemically and chemically quasi-reversible reduction is observed at *ca* -1.375 V *vs* ferrocene, but only after first scanning to potentials beyond that at which the cymantrene core is oxidized. Upon repeat scans (scanning only around the two oxidative processes), the cymantrene oxidation current appears to gradually decrease and then stabilizes after the 10th scan (see Figure S8) whilst the triazole/triazolium redox couple remains stable. However, if repeat scans are performed scanning to more negative potentials than the

couple at -1.375 V, then the cymantrene oxidation current is restored and remains constant over twenty scans.

In order to examine the likely intermediates formed during the complex redox chemistry of our triazole-modified cymantrene complexes, *in situ* infra–red spectroelectrochemistry was performed. The electrode, housed in a specially designed cell was held adjacent to the ATR-IR window of the spectrometer to allow IR characterization of species immediately adjacent to the electrode surface. The experimental set up was verified by first characterizing the spectroelectrochemical shift of the metal–carbonyl peaks of the parent cymantrene, **1**. Reassuringly, both the asymmetric and symmetric stretching modes of the Mn–CO bonds were observed to shift for the $\mathbf{1}^{+\cdot}$ radical cation to larger wavenumbers by *ca.* 100 cm^{-1} replicating Geiger's previous findings.[6] Next a 2 mM yellow solution of **3** was subject to bulk electrolysis, holding the potential at +1.55 V cs. $Fc^{0/+}$ with the IR spectra recorded periodically during the electrolysis. The electrolysis was complete after 30 minutes and the solution had become dark red in color. The IR spectra (Figure 6) reveal that the symmetrical carbonyl stretch at 2030 cm^{-1} gradually decreases in intensity during the electrolysis and shifts by 10 wavenumbers to form a new spectral peak at 2040 cm^{-1} that gradually increased in intensity. A positive shift of 10-20 wavenumbers is also observed for the asymmetric carbonyl stretch, which broadens to form two partially resolved peaks at 1956 and 1965 cm^{-1}. Furthermore, the triazole C=C stretch at 1533 cm^{-1} gradually increased in intensity as the electrolysis proceeded. Increasing the potential electrolytic potential to +2.0 V vs. $Fc^{0/+}$, *i.e.* beyond the second oxidation wave led to the symmetrical carbonyl stretch shifting to higher values by a further 10–15 wavenumbers. However, after 40 minutes of electrolysis at this potential, decomposition of the solution was observed, forming a brown solution with subsequent fouling of the electrode surface.

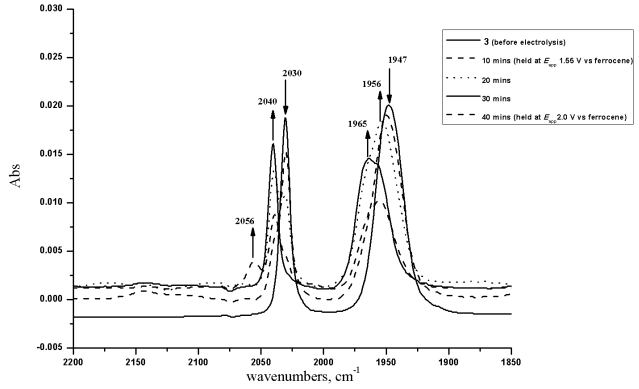

Figure 6. In situ IR spectroelectrochemistry of a bulk solution of 2 mM **3** in CH_2Cl_2/0.1 M $[^nBu_4N][B(C_6F_5)_4]$ at 293 K recorded during bulk electrolysis at E_{app} = 1.55 V.

The magnitude of the shift in the metal carbonyl IR peaks is less than that observed for the parent cymantrene radical cation,[6] and by comparison to other metal–carbonyl–containing systems, this is suggestive of the formation of a dimeric species. In order to probe this further, DFT calculations were performed for neutral **3** and the oxidized radical cation $\mathbf{3}^{+\cdot}$ in both the gas phase and in dichloromethane using a solvent continuum model, to establish the form of the HOMO, LUMO and SOMO, the spin density in the radical cation, and to simulate the predicted IR spectra of the neutral and oxidized forms (see Figures S11 and S12). Comparing the predicted IR spectra of **3** and $\mathbf{3}^{+\cdot}$ (Figure S12) we see that, for the isolated radical cation, $\mathbf{3}^{+\cdot}$, both the symmetric and asymmetric metal–carbonyl stretches are predicted to shift to more positive wave numbers by *ca* 100 cm^{-1} as is observed for the parent cymantrene molecule, whose cation is comparatively stable and long–lived in solution.[6] However, this is not what is observed experimentally, and the reason for this can be seen in the form of the SOMO and the relative spin density of $\mathbf{3}^{+\cdot}$. Geiger reports that for the cymantrene radical cation, $\mathbf{1}^{+\cdot}$, 50% of the spin density resides on the Mn metal centre and 50% on the cyclopentadienyl ligand.[6] However, in the case of $\mathbf{3}^{+\cdot}$ 67% of the spin density resides on the metal in the gas phase, but when modeled in dichloromethane this increases to 97% spin density residing on the metal center, with a large, accessible orbital lobe apparent between the metal–carbonyl groups opposite the pendant triazole moiety (Figure 7). It is therefore, perfectly feasible that, in contrast to the parent cymantrene itself, the electrogenerated $\mathbf{3}^{+\cdot}$ transient intermediate undergoes rapid dimerization in solution to form a Mn–Mn bond, thereby reducing the shift in metal–carbonyl stretches to what is observed experimentally. Note that no evidence for bridging–carbonyl groups is observable. Also note that DFT calculations predict an increase in intensity of the triazole C=C stretch, consistent with that observed experimentally.

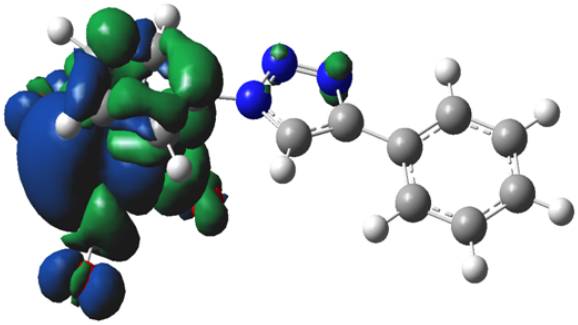

Figure 7. DFT calculated spin density diagram for the SOMO of cationic $\mathbf{3}^+$ in dichloromethane. In the solvent the spin density on the Mn metal centre corresponds to 97% in solvent.

We note that when Geiger first characterized the redox chemistry of cymantrene he reported that the electrogenerated cymantrene radical cation underwent decomposition to produce as yet unidentified redox active products that could be reduced at –0.48 and –1.35 V *vs* ferrocene, as well as evidence of surface adsorbed species leading to electrode fouling.[6] This is similar redox behavior to what we observe for **3** except that, now, with insight from the voltammetric behavior of **3** and **4**, coupled with the results of DFT and spectroelectrochemical infra–red measurements, we tentatively propose that $\mathbf{3}^{+\cdot}$ radical intermediate undergoes some degree of dimerisation to form $\mathbf{3_2}^{2+}$ on the electrode surface. The adsorbed dimer is then reduced at *ca* -0.315 V to form $\mathbf{3_2}^+$ that desorbs and upon further reduction at *ca* -1.375 V fragments to regenerate the parent **3**, Scheme 2A.

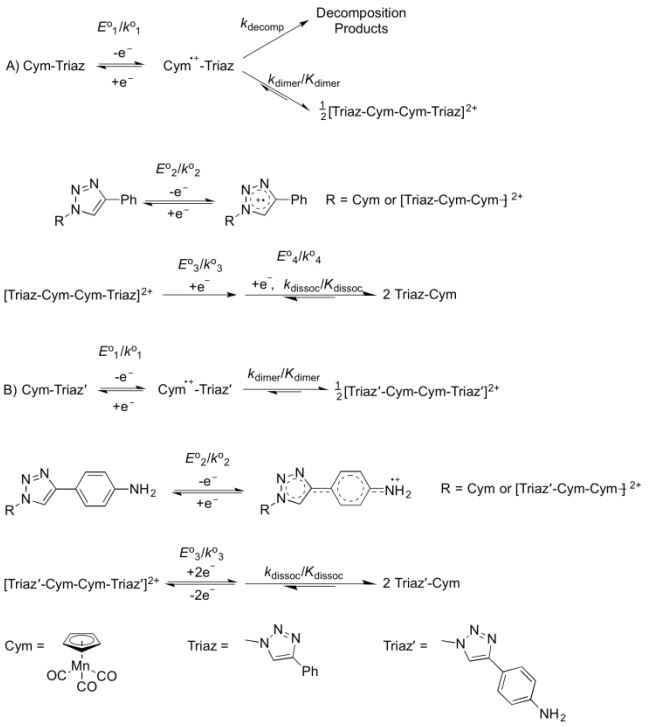

Scheme 2: The proposed mechanism, and associated parameters used in the digital simulation of the cyclic voltammetry of: **A**) compound **3** and **B**) compound **4**.

Digital simulation of cyclic voltammetric data is a powerful tool in determining redox mechanistic electrochemistry. Used correctly, it can provide detailed mechanistic insights – even when proposed intermediates only be transient or not chemically isolable – as well as extracting associated kinetic and thermodynamic parameters, such that the technique offers far more besides simply measuring redox potentials of species under study *vs.* ferrocene. Reassuringly, digital simulation of the observed voltammetry of **3** at varying scan rates (Supporting Information, Figure S9) is consistent with our proposed mechanism in scheme 2A, producing an excellent fit between simulation and experiment. Attempts to fit the simulation to experimental data using a wide variety of other plausible mechanisms, gave much poorer fits outside our confidence value of 95% s.d. Each parameter in the simulation was globally optimized, *i.e.* the simulation converged to a set of values that produced fit to within 95% s.d., across each and every scan rate studied and for each redox peak position, shape and height. Each individual parameter was then varied separately and manually until the simulation no longer produced a satisfactory fit over all redox processes at all scan rates studied, to produce error bounds or minimum lower limiting values. These globally optimized parameters for the redox process and subsequent dimerization processes are given in Table 3. Note that in the case of **3** surface fouling prevented us from quantitatively simulating the triazole/triazolium redox wave using a diffusion-only simulation model.

The solution phase electrochemistry of **4** is much more informative. Again, upon first scanning in an oxidative direction we observe two clear oxidations at *ca* +1.20 V and +1.63 V *vs.* ferrocene, which we once again assign to the oxidation of the cymantrene moiety and the 4-aminophenyl-derivatised triazole ring respectively (Figure 8).

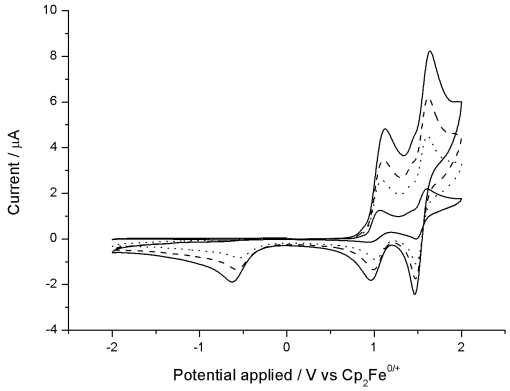

Figure 8. Cyclic voltammogram recorded for 2 mM (η^5-[4-(4-aminophenyl)triazol-1-yl]cyclopentadienyl tricarbonyl manganese(I) **4** in CH_2Cl_2 at varied scan rates; bold line = 2000 mV s^{-1} ; dashed line = 1000 mV s^{-1}; dotted line = 500 mV s^{-1}; 2nd bold line = 100 mV s^{-1}.

Both oxidation potentials appear to be shifted by –200 mV and –145 mV compared to those in **3** and both appear to be more reversible than in the case of **3** at higher scan rates, with corresponding reduction waves observed for both processes. However the reduction wave corresponding to $\mathbf{4}^{+\cdot}$ is approximately half the area (charge) of the oxidation wave when scanned at 2 Vs^{-1}. If the reverse scan is extended into more negative potentials then a clear reduction wave of area again approximately half that of the oxidation of **4** is observed at -0.625 V *vs* ferrocene. The voltammetric behaviour of **4** is strikingly similar to that reported by Geiger for the rhenium analogue, cyrhetrene (η^5–$(C_5H_5)Re(CO)_3$),[31] save for the presence of the triazole/triazolium redox couple. Upon oxidation the cyrhetrene radical cation also undergoes rapid dimersiation, with the dimer reduced at more negative potentials than the parent cyrhetrene. Unlike **3**, complex **4** shows no evidence of surface adsorption onto the electrode, allowing us to fully simulate all redox processes (Figure 9), again invoking the formation of a dimer, with excellent fit between theory and experiment over the scan rates studied (Scheme 2B).

Table 3: Redox parameters, associated chemical equilibria and rate constants determined from digital simulation of CVs for compounds **3** and **4**. [a] Parameter labels are for the appropriate processes as shown in Scheme 2A and B. [b] Optimised values without error ranges shown are reported as the *lower limit* that maintained a good fit between theory and experiment, and beyond which the fit became poor. [c] Modeled as a pseudo-first order process, assuming likely reaction with solvent in large excess. [d] These are potential–dependent equilibrium constants whose values are automatically determined within the simulation by the appropriate values of E^0 for the species involved.

Compound	Standard Potential[a] E^o / V vs. Fc/Fc^+	Electron Transfer Rate Constant[a] k^0 / 10^{-3} cms^{-1}	Charge Transfer Coefficient[a] α	Chemical Step Parameters[a, b]
3	$E^0_1 = +1.37 \pm 0.04$ E^0_2 not simulated $E^0_3 = -0.025 \pm 0.005$ $E^0_4 = -1.30 \pm 0.01$	$k^0_1 = 8.0 \pm 0.2$ ——— $k^0_3 = 1.0 \pm 0.5$ $k^0_4 = 10 \pm 5$	$\alpha_1 = 0.50 \pm 0.05$ ———— $\alpha_3 = 0.20 \pm 0.05$ $\alpha_4 = 0.50 \pm 0.05$	$K_{dimer} = 1.0 \pm 0.1 \times 10^6$ $mol^{-1}dm^3$ $k_{dimer} = 1.0 \pm 0.2 \times 10^4$ $mol^{-1}dm^3s^{-1}$ $k_{decomp} = 5 \pm 1 \times 10^5$ s^{-1} [c] K_{dissoc}[d] $= 8.5 \times 10^{62}$ mol^1dm^{-3} $k_{dissoc} = 1.6 \pm 0.2$ $moldm^{-3}s^{-1}$
4	$E^0_1 = +1.00 \pm 0.02$ $E^0_2 = +1.55 \pm 0.01$ $E^0_3 = -0.40 \pm 0.02$	$k^0_1 = 13 \pm 1$ $k^0_2 = 8.0 \pm 0.1$ $k^0_3 = 2.1 \pm 0.1$	$\alpha_1 = 0.65 \pm 0.05$ $\alpha_2 = 0.55 \pm 0.01$ $\alpha_3 = 0.20 \pm 0.05$	$K_{dimer} = 4.0 \pm 0.2 \times 10^4$ $mol^{-1}dm^3$ $k_{dimer} = 3.00 \pm 0.05 \times 10^3$ $mol^{-1}dm^3s^{-1}$ K_{dissoc}[d] $= 4 \times 10^{43}$ $moldm^{-3}$ $k_{dissoc} = >1 \times 10^9$ $moldm^{-3}s^{-1}$

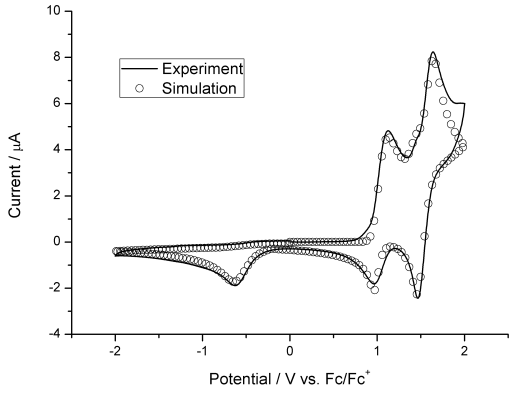

Figure 9. A comparison of experimental (solid line) *vs* simulated data (open circles) for **4** (2mM, in CH_2Cl_2) at a scan rate of $2Vs^{-1}$.

The globally optimized redox parameters obtained from the simulations as well as the equilibrium constant, K_{dimer}, and rate of dimerisation, k_{dimer}, of **4** are included in Table 3. The values of K_{dimer} and k_{dimer} are, respectively, 25 and 3.3 times smaller than those reported by Geiger for cyrhetrene.[31] This likely reflects the tendency of first–row d-block metals, such as Mn, not to form metal-metal bonds as readily as their third–row metal counterparts, *e.g.* Re (although we cannot preclude the possibility that dimerisation of $\mathbf{3}^{+\cdot}$ and $\mathbf{4}^{+\cdot}$ occurs *via* other routes than through metal–metal bonding). We attribute both the shift to less positive redox potentials of **4** compared to **3** and the increased reversibility (chemical stability of the $\mathbf{4}^{+\cdot}$ intermediate) of the redox processes to the resonance stabilization and electron donating character of the 4-amino phenyl moiety on the triazole ring.

The voltammetric characterization of **5** shows two oxidation processes at +1.25 V and +1.55 V *vs* ferrocene (Figure S10). Again, we can assign the first oxidation to the cymantrene moiety. Neither oxidation process appears to be chemically nor electrochemically reversible with broad, ill-defined redox waves observed in the reverse scan. The voltammetry is not reproducible upon repeated scans. This is consistent with the second oxidation wave being due to oxidation of the 3-aminophenyl moiety and/or separately the triazole ring which leads to polymerization and fouling of the electrode surface. This is likely due to the *meta*–-amino group being unable to take part in resonance stabilization and electron donation into the triazole ring to stabilize the radical cation intermediate, unlike the case of **4**, and lends further support to our interpretation of the voltammetry of **4**. The electrode fouling prevents any meaningful attempt at digital simulation of the voltammetric data for **5**.

2.3 Trypanocidal Activity Studies

Recent studies by Nordlander *et al.* have reported various cymantrenyl 4-aminoquinoline conjugate complexes bound together by linking amide bonds or amine linkers, to be active antimalarial complexes. In addition, their compounds showed in some cases submicromolar antitrypanosomal activity against *Trypanosoma brucei*.[3]

Given that triazole-containing molecules have been used on numerous occasions in pharmaceutical drug molecules,[10] and our insight into the potent redox potential of this new class of cymantrene derivatives we next investigated whether cymantrene-triazole complexes **3-5** may exert a similar level of activity against trypanosomal cell lines as those reported by Nordlander.[3] Excitingly, we found that all three click products **3-5** were more active than cymantrene **1** at reducing the growth rate of cells by 50% to that of the controls when tested against *Trypanosoma brucei* (Table 4). The advantage of having a cymantrene spectroelectrochemical redox tag attached to the triazole unit has been pointed out by Geiger,[6] allowing for the possibility of spectroscopic or electrochemical monitoring of the compound in cell cultures, and photochemical activation (release) of the pendant CO groups.

Table 4. [a] MIC = minimal inhibitory concentration, *i.e.*, that concentration of a compound at which all cells were killed. [b] GI_{50} = 50% growth inhibition, *i.e.*, that concentration of a compound necessary to reduce the growth rate of cells by 50% of that of controls. [c] percentage of inhibition at 100 μM

Compound	**MIC[a] (μM)**	**GI_{50}[b] (μM)**
1	∅ >100	∅ >100 (37.0±7.3%)[c]
3	∅ =100	∅ =26.3±1.3
4	∅ =100	∅ =25.2±3.3
5	∅ =100	∅ =27.0±1.2
3-ethynylaniline	∅ >100	∅ >100 (16.7±4.5%)[c]
4-ethynylaniline	∅ >100	∅ =24.6±2.5

3. Conclusions

We have reported the facile synthesis of three new triazole-derivatized cymantrene complexes (**3-5**) in good yield, all of which have been structurally characterized using a variety of techniques. The incorporation of either a *para* or *meta*–amine group into the pendant phenyl ring at the 4-position of the triazole moiety does not adversely affect the "click" reaction used to form it. The effect of adding electron-donating amine groups does have an influence on the redox properties of both the cymantrene core and triazole ring which can be rationalized *via* resonance stabilization of the triazolium intermediate and a decrease in the electron withdrawing effect of the triazole ring on the cyclopentadienyl ligand in the cymantrene core. The use of pendant phenylamine groups proffers opportunities for electrografting of the cymantrene triazole complexes, for applications in electrocatalytic activation of small molecules,[6] and satisfies our conditions for use as a "molecular linker". In contrast to the behavior of the parent cymantrene and its associated radical cation,[6] triazole-derivatised cymantrene complexes show evidence of rapidly forming dimeric species in solution, as evidenced by *in situ* spectroelectrochemical IR data, DFT calculations and digital simulations of voltammetric data. Finally, redox active cymantrene-triazole complexes show reasonable anti–tryponosomal activity at micromolar concentrations compared to the parent cymantrene complex **1**.

Experimental

General Methods. Unless stated otherwise all reagents were purchased from Sigma–Aldrich (Gillingham, UK) and used as supplied with the exception of cymantrene (Strem Chemicals, Cambridge, UK) and 4-ethynylaniline and 3-ethynylaniline (Fluorochem, Derbyshire, UK). *p*-toluenesulfonylazide[32] and cymantrene azide **2**[19,20] were prepared according to literature procedures. All non-aqueous solvents were de-gassed to remove dissolved oxygen and rigorously dried prior to use by distillation under N_2 over the appropriate drying agent: tetrahydrofuran was distilled over sodium benzophenone ketyl; toluene was distilled over sodium wire; dichloromethane and petroleum ether (40/60) were distilled over calcium hydride.

Unless stated otherwise, all reactions were performed under an inert atmosphere of dinitrogen which was pre-dried by passing through columns filled with phosphorous pentoxide and 3Å molecular sieves. Standard Schlenk techniques were employed with a double manifold vacuum line. Solutions were transferred *via* stainless steel cannulas or needles.

^{1}H and ^{13}C NMR spectra were recorded using a Bruker Avance III spectrometer (operating frequency 500.21 MHz for ^{1}H and 125.05 MHz for ^{13}C). Chemical shift values are quoted in parts per million (ppm, δ), and coupling constants J are quoted in Hertz (Hz). High resolution mass spectra (HRMS) were obtained from the service provided by the EPSRC Mass Spectrometry Service at the University of Swansea. HRMS were run on an LTQ Orbitrap XL instrument as solid samples utilizing an ASAP probe. Data were collected using APCl (ionization mode) and FTMS (FT analyzer). Elemental analyses were obtained from the service run at London Metropolitan University utilizing a Carlo Erba Flash 2000 Elemental Analyzer, configured for %CHN. Infrared spectra were acquired using a PerkinElmer μ–ATR Spectrum II spectrophotometer. Solid samples and liquid samples were run neat utilizing the ATR unit of the spectrometer.

Cyclic Voltammetry (CV) was performed using a computer-controlled potentiostat (PGSTAT302N, Autolab, Utrecht, The Netherlands) with a standard three-electrode configuration. CV data were analyzed using the in-built NOVA software. A silver wire (99.99% GoodFellow, Cambridge, UK) served as the pseudo-reference electrode and was calibrated to the ferrocene/ferrocenium redox couple at the beginning and end of each series of experiments as recommended by IUPAC.[33] A platinium coil served as the counter electrode (99.99% Goodfellow, Cambridge, UK). The working electrodes used consisted of platinium macroelectrodes (99.99% Goodfellow, Cambridge, UK) of either 0.5 mm or 0.35 mm diameter. The working electrodes were polished between experiments using successive grades of alumina slurry (1.0–0.1 micron, Kemmet, UK), subjected to a brief period of ultrasonication in distilled water to remove any adhered microparticles, and then placed in a drying–oven prior to use. Cyclic voltammograms were recorded in dry dichloromethane under an inert nitrogen atmosphere using an in-house design of inert atmosphere electrochemical cell maintained at 20 ± 2 ^{0}C. The cells were assembled under inert atmosphere in a nitrogen-filled glovebox (MBraun). [^{n}Bu$_4$N][BArF$_{20}$] was prepared according to the known literature procedure,[34] and used as a supporting electrolyte (0.1 M).[7]

Anti-trypanosomal activity assay: Bloodstream forms of *T. brucei* clone 427-221a[35] were grown in Baltz medium[36] supplemented with 16.7% heat-inactivated foetal calf serum at 37°C in a humidified atmosphere containing 5% CO_2. Toxicity assays were performed as previously described.[37] In brief, trypanosomes (10^4/ml) were seeded in 24-well plates in a final volume of 1 ml culture medium containing various concentrations of test compounds dissolved in 100% DMSO. The controls contained DMSO alone. In all experiments, the final DMSO concentration was 1%. After 24 h incubation, 100 μl resazurin solution (11.11 mg resazurin sodium salt in 100 ml PBS) were added and the trypanosomes were incubated for a further 48 h. Then, the plates were read on a microplate reader using a test wavelength of 570 nm and a reference wavelength of 630 nm. The 50% growth inhibition (GI_{50}) values, i.e. the concentration of compounds necessary to reduce the growth rate of cells by 50% to that of controls, was determined by linear interpolation according to the method described by Huber and Koella.[38] The minimum inhibitory concentration (MIC) values, i.e. the concentration of the compounds at which all cells were killed, was determined microscopically.

***p*-Toluenesulfonylazide:**[32] A solution of *p*-toluenesulfonylchloride (9.5 g, 49.7 mmol) in acetone (25 mL) was added to a stirred solution of sodium azide (3.6 g, 55.4 mmol) in water (15 mL). The solution was allowed to stir for 2 h at ambient temperature. The reaction mixture was concentrated under reduced pressure, the residue extracted with dichloromethane (50 mL) and dried over $MgSO_4$. Removal of volatiles at reduced pressure afforded **2** as a colorless oil (7.35 g, 75%). ^{1}H NMR (500 MHz, $CDCl_3$): δ 7.80 (d, 2H, J = 8 Hz), 7.38 (d, 2H, J = 8 Hz), 2.45 (s, 3H). ^{13}C NMR (125 MHz, $CDCl_3$): 146.3, 135.4, 130.3, 127.4, 21.7

Cymantrene azide CymN$_3$ 2:[19] To a cold (-78°C) solution of cyclopentadienylmanganese tricarbonyl **1** (1.0 g, 4.9 mmol) in 50 mL of THF was added 1.6 M solution of *n*-BuLi in hexanes (3.1 mL, 4.9 mmol), and the reaction mixture left to stir at -78°C for 2 h. A solution of *p*-toluenesulfonylazide (1.0 g, 4.9 mmol) dissolved in THF (50 mL) was then added *via* cannula dropwise to the stirred solution over a period of 10 minutes. The resultant orange solution was allowed to warm to room temperature for 13 h in the dark. Removal of remaining solvents under reduced pressure afforded the thermally unstable cymantrenyl azide **2** (Caution! Care should be taken during the preparation of such potentially explosive organometallic azides, especially on scaled up reactions) as a light brown solid (0.78 g, 65%), which was used without further purification. ATR-FT IR ν_{max} / cm^{-1}; 2120 (ν_{NN}), 2016 (ν_{CO}), 1910 (ν_{CO}). ^{1}H NMR (500 MHz, CD_2Cl_2): δ 4.67 (t, 2H, J = 2 Hz), 4.74 (t, 2H, J = 2 Hz) (75:25 ratio of **2**:**1** – residual **1** at 4.78 ppm, s). ^{13}C NMR (125 MHz, CD_2Cl_2): *d* 72.9 (2C), 80.4 (2C), 116.8 (C *quat.*) (residual **1** at 84.0 ppm).

(η^5-[4-phenyltriazol-1-yl]cyclopentadienyl tricarbonyl manganese(I) 3:[24] To a solution of crude cymantrenyl azide **2** (0.25 g, 1.0 mmol) in acetonitrile (10 mL) was added phenylacetylene (0.1 g, 1.0 mmol) and $Cu(OAc)_2 \cdot H_2O$ (0.02 g, 0.1 mmol) and stirred at ambient temperature under a nitrogen atmosphere. Reaction progress was monitored by thin layer chromatography, and upon completion solvents were removed under reduced pressure. The residue was purified directly using silica gel flash column chromatography (petroleum ether 60/40: acetone, 15:2) yielding **3** as a fine yellow solid. Slow recrystallization of **3** from petroleum ether:dichloromethane (50:50) afforded single colorless plates suitable for X-ray crystallography (0.29 g, 83%). ATR-FT IR ν_{max} / cm^{-1}; 3130, 2025 (ν_{CO}), 1959 (ν_{CO}), 1936 (ν_{CO}), 1918 (ν_{CO}), 1534 ($\nu_{C=C}$), 1453, 1232. ^{1}H NMR (500 MHz, CD_2Cl_2): δ 7.99 (s, 1H), 7.85 (d, 2H, J = 8 Hz), 7.47 (t, 2H, J = 8 Hz), 7.38 (t, 1H, J = 8 Hz), 5.48 (t, 2H, J = 2 Hz), 4.86 (t, 2H, J = 2Hz). ^{13}C NMR (125 MHz, CD_2Cl_2): δ 148.8, 130.3, 129.5 (2C), 129.2, 126.3 (2C), 118.9, 108.1, 80.8 (2C), 75.4 (2C). Anal. calcd for $C_{16}H_{10}MnN_3O_3$: C, 55.35; H, 2.90; N, 12.10; Found: C, 55.27; H, 3.05; N, 11.95. HRMS (ASAP): $[C_{16}H_{10}MnN_3O_3 + H]^+$ requires 348.0175; Found 348.0174 $[M+H]^+$.

((η⁵-[4-(4-aminophenyl)triazol-1-yl]cyclopentadienyl tricarbonyl manganese (I) 4:[24,26] To a solution of cymantrenyl azide **2** (0.75 g, 3.0 mmol) in acetonitrile (30 mL) was added 4-ethynylaniline (0.36 g, 3.0 mmol) and $Cu(OAc)_2 \cdot H_2O$ (0.06 g, 0.3 mmol) and stirred at ambient temperature under a nitrogen atmosphere. Reaction progress was monitored by thin layer chromatography, and upon completion solvents were removed under reduced pressure. The residue was purified directly using silica gel flash column chromatography (petroleum ether 60/40: acetone, 4:1) yielding **4** as a fine yellow powder (0.81 g, 75%). ATR-FT IR ν_{max} / cm^{-1}; 3406 (ν_{NH}), 3109, 2022 (ν_{CO}), 1940 (ν_{CO}), 1910 (ν_{CO}), 1621($\nu_{C=C}$), 1566 ($\nu_{C=C}$), 1540 ($\nu_{C=C}$), 1499, 1264. ^{1}H NMR (500 MHz, $CDCl_3$): δ 7.77 (s, 1H), 7.65 (s, 2H), 6.75 (s, 2H), 5.41 (s, 2H), 4.80 (s, 2H), 3.82 (bs, 2H). ^{13}C NMR (125 MHz, $CDCl_3$): δ 149.0, 147.2, 127.3 (2C), 120.0, 116.8, 115.4 (2C), 107.9, 80.0 (2C), 74.5 (2C). Anal. calcd for $C_{16}H_{11}MnN_4O_3$: C, 53.05; H, 3.06; N, 15.47; Found: C, 53.19; H, 2.97; N, 15.34. HRMS (ASAP): $[C_{16}H_{11}MnN_4O_3 + H]^+$ requires 363.0284; Found 363.0282 $[M+H]^+$

((η⁵-[4-(3-aminophenyl)triazol-1-yl]cyclopentadienyl tricarbonyl manganese (I) 5:[24,26] To a solution of cymantrenyl azide **2** (0.20 g, 0.8 mmol) in acetonitrile (10 mL) was added 3-ethynylaniline (0.10 g, 0.8 mmol) and $Cu(OAc)_2 \cdot H_2O$ (0.02 g, 0.08 mmol) and stirred at ambient temperature under a nitrogen atmosphere. Reaction progress was monitored by thin layer chromatography, and upon completion solvents were removed under reduced pressure. The residue was purified directly using silica gel flash column chromatography (petroleum ether 60/40: acetone, 7:1) yielding **5** as a dark yellow oil (0.12 g, 41%). Slow recrystallization of **5** from petroleum ether:dichloromethane afforded single colorless crystals. ATR-FT IR ν_{max} / cm^{-1}; 3361 (ν_{NH}), 3117, 2925, 2022 (ν_{CO}), 1928 (ν_{CO}), 1615, 1592, 1530, 1481, 1159. ^{1}H NMR (500 MHz, CD_2Cl_2): δ 7.93 (s, 1H), 7.16-7.23 (m, 3H), 6.69 (m, 1H), 5.46 (s, 2H), 4.85 (s, 2H), 3.84 (bs, 2H). ^{13}C NMR (125 MHz, $CDCl_3$): δ 149.0, 148.0, 131.1, 130.4, 118.9, 116.3, 115.7, 112.5, 108.2, 80.8 (2C), 75.3 (2C). Anal. calcd for $C_{16}H_{11}MnN_4O_3$: C, 53.05; H, 3.06; N, 15.47; Found: C, 52.88; H, 2.90; N, 15.35. HRMS (ASAP): $[C_{16}H_{11}MnN_4O_3 + H]^+$ requires 363.0284; Found 363.0281 $[M+H]^+$.

Supporting Information. ^{1}H– and ^{13}C–NMR characterization data for compounds **2**–**5**. Comparison of digital simulation and experimental cyclic voltammograms of **3**-**5**. Tabulated crystal data, collection and refinement parameters, bond distances, and angles for **3** and **5** in CIF format. DFT computational details, calculated molecular orbitals of **3** and $\mathbf{3}^{+\cdot}$ in the gas phase and in solution, and predicted IR spectra of species in the gas phase and solution. This material is available free of charge *via* the Internet at http://pubs.acs.org

Corresponding Author
*Gregory G. Wildgoose; Email: G.Wildgoose@uea.ac.uk

Acknowledgements

The research leading to these results has received funding from the European Research Council under the European Union's ERC Grant Agreement n°. ERC–StG–307061 PiHOMER. GGW thanks the Royal Society for additional support *via* a University Research Fellowship. TD thanks the University of East Anglia for financial support *via* a Dean's studentship.

Refrences

(1) (a) Calladine, J. A.; Duckett, S. B.; George, M. W.; Matthews, S. L.; Perutz, R. N.; Torres, O.; Vuong, K. *J. Am. Chem. Soc.* **2011**, 133, 2303-2310. (b) To, T. T.; Duke III, C. B.; Junker, C. S.; O'Brien, C. M.; Ross II, C. R.; Barnes, C. E.; Webster, C. E.; Burkey, T. J. *Organometallics* **2008**, *27*, 289-296

(2) Kee, J. W.; Tan, Y. Y.; Swennenhuis, B. H. G.; Bengali, A. A.; Fan, W .Y. *Organometallics*, **2011**, *30*, 2154-2159

(3) Glans, L.; Hu, W.; Jöst, C.; de Kock, C.; Smith, P. J.; Haukka, M.; Bruhn, H.; Schatzschneider, U.; Nordlander, E. *Dalton Trans.*, **2012**, *41*, 6443-6450

(4) Dallagi, T.; Saidi, M.; Jaouen, G.; Top, S. *Appl. Organometal. Chem.*, **2013**, *27*, 28-35

(5) Geiger, W. E. *Coordination Chemistry Reviews*, **2013**, *257*, 1459-1471

(6) Laws, D. R.; Chong, D.; Nash, K.; Rheingold, A. L.; Geiger, W. E. *J. Am. Chem. Soc.*, **2008**, *130*, 9859-9870

(7) Geiger, W. E.; Barrière, F. *Accounts Chem. Res.* **2010**, *43*, 1030-1039

(8) Laws, D. R.; Sheats, J.; Rheingold, A. L.; Geiger, W. E. *Langmuir.*, **2010**, *26*, 15010-15021

(9) Huisgen, R. in *1,3-Dipolar Cycloadditional Chemistry* (Ed.: A.Padwa), Wiley, New York, **1984**

(10) For the most comprehensive reviews on Click chemistry see; (a) Kolb, H. C.; Finn, M. G.; Sharpless, K. B. *Angew. Chem. Int. Ed.*, **2001**, *40*, 2004-2021. (b) Bock, V. D.; Hiemstra, H.; van Maarseveen, J. H. *Eur. J. Org. Chem.*, **2006**, 51-68. (c) Gil, M. V.; Arévalo, M. J.; López, Ó. *Synthesis.*, **2007**, *11*, 1589-1620. (d) Kolb, H. C.; Sharpless, K. B. *Drug Discov. Today.*, **2003**, *8*, 1128–1137

(11) (a) Anderson, C. B.; Elliott, A. B. S.; McAdam, C. J.; Gordon, K. C.; Crowley, J. D. *Organometallics,* **2013**, *32*, 788-797. (b) Kilpin, K. J.; Gavey, E. L.; McAdam, C. J.; Anderson, C. B.; Lind, S. J.; Keep, C. C.; Gordon, K. C.; Crowley, J. D. *Inorg. Chem.* **2011**, *50*, 6334-6346

(12) (a) Beyer, B.; Ulbricht, C.; Escudero, D.; Friebe, C.; Winter, A.; González, L.; Schubert, U. S. *Organometallics,* **2009**, *28*, 5478-5488. (b) Happ, B.; Escudero, D.; Hager, M. D.; Friebe, C.; Winter, A.; Görls, H.; Altuntas, E.; González, L.; Schubert, U. S. *J. Org. Chem.* **2010**, *75*, 4025-4038

(13) (a) Schweinfurth, D.; Demeshko, S.; Khusniyarov, M. M.; Dechert, S.; Gurram, V.; Buchmeiser, M. R.; Meyer, F.; Sarkar, B. *Inorg. Chem.* **2012**, *51*, 7592-7597. (b) Schweinfurth, D.; Weisser, F.; Bubrin, D.; Bogani, L.; Sarkar, B. *Inorg. Chem.* **2011**, *50*, 6114-6121. (c) Schweinfurth, D.; Krzystek, J.; Schapiro, I.; Demeshko, S.; Klein, J.; Telser, J.; Ozarowski, A.; Su, C.-Y.; Meyer, F.; Atanasov, M.; Nesse, F.; Sarkar, B. *Inorg. Chem.* **2013**, *52*, 6880-6892

(14) (a) Romero, T.; Orenes, R. A.; Espinosa, A.; Tárraga, A.; Molina, P. *Inorg. Chem.* **2011**, *50*, 8214-8224. (b) Otón, F.; González, M. C.; Espinosa, A.; Ramírez de Arellano, C.; Tárraga, A.; Molina, P. *J. Org. Chem.* **2012**, *77*, 10083-10092. (c) Romero, T.; Caballero, A.; Tárraga, A.; Molina, P. *Org. Lett.* **2009**, *11*, 3466-3469. (d) Otón, F.; González, M. C.; Espinosa, A.; Tárraga, A.; Molina, P. *Organometallics* **2012**, *31*, 2085-2096. (e) Romero, T.; Orenes, R. A.; Tárraga, A.; Molina, P. *Organometallics* **2013**, Article ASAP, DOI: 10.10211om4002457

(15) (a) Ornelas, C.; Aranzaes, J. R.; Salmon, L.; Astruc, D. *Chem. Eur. J.* **2008**, *14*, 50-64. (b) Ornelas, C.; Aranzaes, J. R.; Cloutet, E.; Alves, S.; Astruc, D. *Angew. Chem. Int. Ed.* **2007**, *46*, 872-877. (c) Astruc, D.; Ornelas, C.; Aranzaes, J. R. *Acc. Chem. Res.* **2008**, *41*, 841-856. (d) Badèche, S.; Daran, J.-C.; Ruiz, J.; Astruc, D. *Inorg. Chem.* **2008**, *47*, 4903-4908.

(16) Rapakousiou, A.; Wang, Y.; Belin, C.; Pinaud, N.; Ruiz, J.; Astruc, D. *Inorg. Chem.* **2013**, *52*, 6685-6693

(17) Clough, M. C.; Zeits, P. D.; Bhuvanesh, N.; Gladysz, J. A. *Organometallics*, **2012**, *31*, 5231-5234

(18) Sheridan, M. V.; Lam, K.; Geiger, W. E. *J. Am. Chem. Soc.* **2013**, *135*, 2939-2942

(19) Holovics, T. C.; Deplazes, S. F.; Toriyama, M.; Powell, D. R.; Lushington, G. H.; Barybin, M. V. *Organometallics* **2004**, *23*, 2927-2938

(20) Sünkel, K.; Birk, U.; Soheili, S.; Stramm, C.; Teuber, R. *J. Organomet. Chem.* **2000**, *599*, 247-255

(21) Leroux, Y. R.; Hui, F.; Noël, J.-M.; Roux, C.; Downard, A. J.; Hapiot, P. *Langmuir* **2011**, *27*, 11222-11228

(22) (a) Evrard, D.; Lambert, F.; Policar, C.; Balland, V.; Limoges, B. *Chem. Eur. J.* **2008**, *14*, 9286-9291. (b) Leroux, Y. R.; Fei, H.; Noël, J.-M.; Roux, C.; Hapiot, P. *J. Am. Chem. Soc.* **2010**, *132*, 14039-14041

(23) Attempts at purifying **2** either by recrystallization or by silica gel column chromatography led to the decomposition of the inorganic azide on both occasions

(24) Liu, Y.; Wang, X.; Xu, J.; Zhang, Q.; Zhao, Y.; Hu, Y. *Tetrahedron* **2011**, *67*, 6294-6299

(25) (a) Lunquist, R. T.; Cais, M. *J. Org. Chem.***1962**, *27*, 1167-1172. (b) Lage, M. L.; Curiel, D.; Fernández, I.; Mancheño, M. J.; Gómez-Gallego, M.; Molina, P.; Sierra, M. A. *Organometallics*, **2011**, *30*, 1794-1803

(26) Yoo, E. J.; Ahlquist, M.; Kim, S. H.; Bae, I.; Fokin, V. V.; Sharpless, K. B.; Chang, S. *Angew. Chem. Int. Ed.* **2007**, *46*, 1730-1733

(27) Borissova, A. O.; Antipin, M. Y.; Lyssenko, K. A. *J. Phys. Chem. A.* **2009**, *113*, 10845-10851

(28) Carvalho, I.; Andrade, P.; Campo, V. L.; Guedes, P. M. M.; Sesti-Costa, R.; Silva, J. S.; Schenkman, S.; Dedola, S.; Hill, L.; Rejzek, M.; Nepogodiev, S. A.; Field, R. A. *J. Bioorg. Med. Chem.* **2010**, *18*, 2412-2427

(29) Hirano, T.; Kubo, H.; Shiraishi, T.; Hiromoto, K.; Fujiwara, T.; Kagechika, H. *Tetrahedron Lett.*, **2012**, *53*, 5916-5919

(30) Abboud, J.-L. M.; Concepción, F.-F.; Notario, R.; Trifonov, R. E.; Volovodenko, A. P.; Ostrovskii, V. A.; Alkorta, I.; Elguero, J. *Eur. J. Org. Chem.* **2001**, *2001*, 3013-3024

(31) Chong, D.; Laws, D. R.; Nafady, A.; Costa, P. J.; Rheingold, A. L.; Calhorda, M. J.; Geiger, W. E. *J. Am. Chem. Soc.* **2008**, *130*, 2962-2703

(32) Jaschinski, T.; Hiersemann, M. *Org. Lett.* **2012**, *14*, 4114-4117

(33) Gritzner, G.; Kůta, J. *Electrochimica Acta* **1984**, *29*, 869-873

(34) Lawrence, E. J.; Oganesyan, V. S.; Wildgoose, G. G.; Ashley, A. E. *Dalton Trans.* **2012**, *42*, 782-789

(35) Hirumi, H.; Hirumi, K.; Doyle, J. J.; Cross, G. A. M. *Parasitology* **1980**, 80, 371-382

(36) Baltz, T.; Baltz, D.; Giroud, C.; Crockett, J. *EMBO J.* **1985**, 4, 1273-1277

(37) Steverding, D.; Wang, X. *Parasit. Vectors* **2009**, 2, 29

(38) Huber, W.; Koella, J. C. *Acta Trop.* **1993**, 55, 257-262

SYNOPSIS TOC